Published in final edited form as:
Nat Geosci. 2017 October ; 10(10): 783–787. doi:10.1038/ngeo3032.

Magmatic pulse driven by sea-level changes associated with the Messinian salinity crisis

Pietro Sternai[1,*], **Luca Caricchi**[1], **Daniel Garcia-Castellanos**[2], **Laurent Jolivet**[3,†], **Tom E. Sheldrake**[1], and **Sébastien Castelltort**[1]

[1]Department of Earth Sciences, University of Geneva, Geneva, Switzerland [2]Instituto de Ciencias de la Tierra Jaume Almera, ICTJA-CSIC, Barcelona, Spain [3]Intitut des Sciences de la Terre d'Orléans, University of Orléans, Orléans, France

Abstract

Between 5 and 6 million years ago, during the so-called Messinian salinity crisis, the Mediterranean basin became a giant salt repository. The possibility of abrupt and kilometre-scale sea-level changes during this extreme event is debated. Messinian evaporites could signify either deep- or shallow-marine deposits, and ubiquitous erosional surfaces could indicate either subaerial or submarine features. Significant and fast reductions in sea level unload the lithosphere, which can increase the production and eruption of magma. Here we calculate variations in surface load associated with the Messinian salinity crisis and compile the available time constraints for pan-Mediterranean magmatism. We show that scenarios involving a kilometre-scale drawdown of sea level imply a phase of net overall lithospheric unloading at a time that appears synchronous with a magmatic pulse from the pan-Mediterranean igneous provinces. We verify the viability of a mechanistic link between unloading and magmatism using numerical modelling of decompression partial mantle melting and dike formation in response to surface load variations. We conclude that the Mediterranean magmatic record provides an independent validation of the controversial kilometre-scale evaporative drawdown and sheds new light on the sensitivity of magmatic systems to the surface forcing.

Local- or regional-scale magmatic activity has been linked to modifications of the environmental conditions, either by driving climate changes [1] or in response to surface load variations due to glacio-eustatic changes [2,3,4,5,6,7]. The Mediterranean Messinian salinity crisis (MSC), occurred between ~5.97-5.33 Ma (ref. [8]) due to the temporary closure of the

Correspondence and request for material should be addressed to P.S. (pietro.sternai@unige.ch; pietrosternai@yahoo.it).
[†]Now at the University Pierre et Marie Curie (UPMC-Paris VI), Paris, France

Author contributions

PS conceived the scientific question, designed and performed the work and wrote the manuscript. LC contributed to the conception of the scientific question and helped with the MELTS modeling. DGC and LJ provided fundamental insights into the available knowledge about the MSC as well as the Mediterranean geodynamics and magmatism. TS helped with the statistical treatment of data. SC contributed to the conception of the scientific question. All authors contributed to the design of the work and improved the manuscript.

Competing financial interests

The authors declare no competing financial interests.

Europe PMC Funders Author Manuscripts

straight of Gibraltar, resulted in the formation of thick evaporitic layers in the deep basin and inland 9,10,11 and involved a combination of environmental and eustatic changes that may also have influenced the regional magmatism. However, while the occurrence of an intra-MSC sea level lowering is widely accepted today 12, questions remain about the magnitude and modalities of the desiccation 13,14. This controversy stems from the discovery of deep fluvial incision extending from the Mediterranean into the Eurasian and African continents 15 leading to discussions regarding the shallow or deep marine deposition of the Messinian evaporites 16,17.

Surface load variations due to the MSC and igneous record

In order to investigate the potential impact of the MSC on Mediterranean magmatism, we calculate the overall surface load variations associated with sea level and water density changes as well as the formation of salt deposits (Methods). We first test the scenario proposed by ref. 18 (Fig. 1a), based on both direct and geophysical observations and conveniently covering the entire Mediterranean. According to this model, lithospheric loading occurs during the early MSC due to increased water salinity and limited evaporative drawdown and salt deposition (Fig. 1b). The contribution to surface load variations by salt deposition should be reduced by 50% to 75% in order to account for the interleaved sediment 18. As a result, during the late-MSC, the unloading due to the drawdown overcomes the loading by increased water density and salt deposition by up to ~15 and ~10 MPa, on average, in the eastern and western Mediterranean, respectively. These estimates are highly conservative as they do not account for erosion both onshore and on present-day shelves and slopes 15,19, which implies additional lithospheric unloading synchronous and prior to the evaporative drawdown of the brine surface 20.

To compare these results with regional magmatic trends we count the number of intrusive and effusive events from the pan-Mediterranean igneous provinces during the Neogene, based on published igneous mineral ages (Methods, Supplementary Table 1). During the late-MSC a gross but concrete magmatic pulse, significant at the ~95% confidence level, is observed (Fig. 1c, d). Such a late-MSC peak magmatism is widespread but particularly concerns the eastern Mediterranean, where the salt is distributed over a larger area and, according to the reference MSC scenario 18, the drawdown is more significant (Fig. 1a). The short-lived late-MSC increase in magmatism, in addition, cannot be justified by significant changes of overall geodynamics 21 (Methods and Supplementary Fig. 1). The correspondence between the recognized magmatic pulse and the estimated net lithospheric unloading during the late-MSC is striking (Fig. 1a-c), suggesting that the intra-MSC drawdown enhanced active magmatic processes, which include partial mantle melting by adiabatic decompression and dike formation 22,23,24 (more detail below).

We also explore two alternative loading/unloading scenarios (Supplementary Fig. 2). The first involves an earlier and shorter timing for the intra-MSC drawdown and shallow-marine salt deposition as suggested by seismic surveys and field observations from the Gulf of Lions, Italy and Turkey 25. The second assumes the deep-waters formation of the Messinian evaporites in absence of significant drawdown 13,14. In the first case, considerable net average lithospheric unloading still occurs and is largely synchronous with the magmatic

pulse. Conversely, the deep-water scenario for the formation of the Messinian evaporites implies net average lithospheric loading during the entire MSC, which is, based on the principles that we explore hereafter, at odds with the recognized magmatic trends.

Effects of the MSC on magma production and dike formation

The following quantitative assessments inherent to the geodynamic context provide independent support to the existence of a causative link between the estimated MSC-related surface load variations and the regional magmatic trends. Since at least the Oligocene, the Africa-Eurasia convergence and rollback of subducting slabs characterize the Mediterranean geodynamics 21, while partial melting by adiabatic decompression of hydrated mantle rocks across extensional back-arc domains controls the bulk of the regional magmatism 22,23,24 (see also Methods). Back-arc spreading occurred at rates up to a few cm/a (ref. 21), causing parcels of mantle to flow upward at similar rates. Such upwelling leads to a background geodynamic decompression of rising mantle rocks in the order of the hundreds of Pa/a. Our geodynamic numerical models (Methods) suggest that pressure changes at depth in response to the MSC-related surface load variations vary in the order of the tens of Pa/a and may reach up to one order of magnitude higher during extreme events (Fig. 2). These values also apply to modelled pressure changes below the edges of the basin-like structure, representative of regions where most observations reporting on the Mediterranean magmatism are found (Fig. 1 and Supplementary Table 1). Hence, MSC-related surface load variations would modify the background geodynamic depressurization rates by a minimum amount of ~10 %.

Assessing the corresponding effects on the volumes of magma produced is difficult, especially because quantitative constraints on the Mediterranean thermo-chemical structure during the MSC are lacking. Assuming uniform and constant mantle upwelling and density, however, the modulation in melt production rate due to surface load changes scales linearly with their modification of the pressure change rate in the mantle (see Methods, equations (4-6)). In Fig. 3a, we consider an equilibrium continental geothermal structure and a parameterization for partial mantle melting as function of pressure and temperature 26. In Fig. 3b we show the degree of partial melting at depth and, in Fig. 3c, the melt production rate at equilibrium conditions is increased by an amount equivalent to that associated with the relative modification of the depressurization rates by the MSC-related surface unloading shown in Fig. 2c, along the vertical through the reference point. We found an increase in the depth-integrated melt production rate (i.e., additional melt) per unit surface area by ~17 % during the unloading phase of the reference MSC scenario. In the case of surface unloading where the depth-integrated amount of melts measures 6 km, this translates into the approximate production of an additional km^3 of melts for each squared km subject to unloading, only due to the surface forcing. This estimate is conservative considering that the portion of partially molten Mediterranean mantle is in many places thicker than 6 km (ref. 27) and that the Messinian geothermal structure of the Mediterranean back-arc regions was likely hotter than the equilibrium state considered here.

The rate of upward percolation of the mantle melts with respect to the solid matrix determines the time lag between the production and the eruption/emplacement of magma.

This quantity primarily depends on the lithosphere and asthenosphere permeability. Because the igneous activity of the magmatic provinces in Fig. 1d was initiated prior to the MSC 22,28,24,23, one can assume that the vertical connections of channels along the solid matrix grain boundaries were already established. Under this assumption and according to the porous flow model proposed by refs. 29,30, the vertical migration velocity of the magma varies in the order of tens of meters per year, which implies that a considerable amount of newly-produced magma would reach shallow crustal reservoirs (or be erupted) within a few tens of thousands of years after the MSC-related unloading phase. However, such a time lag can increase considerably if, for instance, the deformation and collapse of the solid matrix is not sufficiently rapid to provide the vertical connections of channels along grain boundaries or depending on the viscosity and density of the melts with respect to those of the matrix 30.

At shallower levels, the overpressure within crustal magma reservoirs, $\Delta P_{ch} = P_{ch} - P_r$ (where P_{ch} is the pressure within the reservoir and P_r is the remote lithostatic stress), affects the frequency and explosivity of volcanic eruptions 3. Increased magma fluxes can increase P_{ch}, while surface load variations control the tensile deviatoric stresses required to dilate fractures by modulating P_r, inhibiting or facilitating dike formation when loading or unloading, respectively, take place. According to the model presented in ref. 3 (Methods), the elastic instantaneous response of a magmatic system is proportional to the rates of surface load changes. We remark that, regardless of the MSC scenario that is considered, MSC-related loading/unloading rates (e.g., Fig. 1b, and Supplementary Fig. 2) are considerably higher than during Quaternary glacioeustatic changes, which have been proven capable of affecting the Mediterranean volcanism 7.

In Fig. 4a, we show the computed overpressure time history within a hypothetical magma chamber at 20 km depth based on the analytical framework provided by ref. 3 (see Methods, equations (7) and (8)) and the pressure changes at depth from our geodynamic models (Fig. 2). Such a calculation shows that the estimated surface unloading related to MSC scenarios involving a km-scale sea-level drawdown (e.g., Fig. 1a, b) can enhance the overpressure within the magma chamber, thereby increasing the likelihood of dike formation. This effect would be even more pronounced if the drop in sea level was of similar magnitude but occurred faster (e.g., the MSC scenario in Supplementary Fig. 2), for the rate-of-change of surface load is the leading-order factor controlling the magmatic response in terms of dike formation. It is also noteworthy that, besides the effects on ΔP_{ch} due to modulations of P_r, the MSC-related surface loading or unloading may respectively lead to horizontal compressional or extensional deviatoric stresses at crustal levels (Fig. 4b, c and Supplementary Fig. 3), which can further inhibit/help the nucleation and propagation of dikes 31. Eruptions by overpressure and dike formation due to the MSC-related surface load variations should be delayed by ~10 ka because of the partly viscous rock rheology 3. Yet, such a delay is short enough to allow us to relate the observed regional magmatic pulse to the net average unloading of the Mediterranean lithosphere during the late-MSC.

Increased magmatic activity appears associated with melting of ice-sheets and erosion across thickened continental lithospheres 4,6,3. The MSC implies a similar surface forcing but on the Mediterranean basin, which is atop of a lithosphere that has been subject to widespread thinning and warming since at least the Oligocene 21. We thus propose that the net mean

lithospheric unloading during the late-MSC is a likely cause behind the synchronous pulse of the Mediterranean magmatism derived from available geochemical data. Given the volume of Messinian evaporites, however, only scenarios involving a km-scale sea-level fall 9,25,18 can explain the magmatic pulse by the mechanisms proposed here. While this does not rule out the precipitation of the Messinian evaporites under a significant water column, it does point toward their formation in a partially desiccated Mediterranean basin. Our study also provides support to the vision that the melting of the solid Earth is highly sensitive to the surface forcing 5,4,6, greatly advancing ongoing debates 5,32. More data and work in this novel direction are warranted and could, for instance, allow distinguishing between either multiple short intra-MSC desiccations 33 or a long lasting shallow Mediterranean-Atlantic connection 34. In any case, we anticipate that the environmental changes associated with the MSC had far bigger effects on the Mediterranean magmatism than have been proposed thus far.

Methods

Mediterranean geodynamic and magmatic context

The geodynamic and magmatic evolution of the Mediterranean during the Cenozoic is controlled by the Africa-Eurasia convergence and the associated collisional and subduction dynamics (Supplementary Fig. 1). Since the late-Oligocene, the collision between Africa and Eurasia in the Betic cordillera and the Rif as well as in the Hellenides and Taurides constrained the Mediterranean subductions in the east and west, respectively 35. As a result, rollback of the subducting slabs became predominant and led to the opening of the major back-arc basins that shape the present-day physiography of the Mediterranean: the Alboran Sea, the Liguro-Provençal basin, the Tyrrhenian Sea and the Aegean Sea. During the Messinian, probably due to the narrow space available for slab retreat, limited back-arc extension is observed in the Alboran Sea 36. Conversely, back-arc extension related to slab rollback developed since the early-Miocene in the internal Apennines and the northern Tyrrhenian Sea 37 and progressively migrated eastward through time 38. Similarly, following the late-Oligocene collisional events, the Aegean back-arc extension migrated regularly southward due to ongoing rollback of the Hellenic slab 23.

Neogenic magmatic rocks in the westernmost Mediterranean, which provide debated clues on the origins of the MSC 39,22,21, are found onshore and offshore along a NE-SW trending lineament across the Alboran Sea and the western Betics. A transition toward shoshonites and alkali basalts, largely synchronous with the MSC, in particular, is interpreted as the shift from subduction-related to intra-plate magmatism due to slab detachment and associated asthenospheric mantle upwelling and decompression-melting 22. The magmatic activity in the Tyrrhenian Sea accompanies the eastward migration of the back-arc extension 28 and is predominantly characterized by granitoids intrusives and associated volcanic products 24. Also the Aegean magmatism migrated regularly southward, following the back-arc extensional domain migration, to reach its present-day position 23. Despite the unusual range of chemistry and petrology, the overall Aegean picture is compatible with arc and back-arc magmatism 40. Since the middle-Miocene, slab tearing below western Turkey and the associated toroidal and upwelling mantle flow controlled the

intense regional tectonics and magmatism 23,41,42,43. The bulk of the late-Cenozoic Mediterranean magmatism, thus, appears to be related to decompression partial melting of upwelling mantle rocks due to slab detachment and/or stretching of the upper plate.

Estimates of surface load variations during the MSC

Our reference MSC scenario is provided by ref. 18 (Fig. 1a), that models the magnitude and timing of the sea level variations, water salinity and salt deposition during the MSC based on the physical laws controlling the water exchange between the Atlantic and the Mediterranean. The volumes of the evaporites and the Mediterranean paleo-climate and paleo-hypsometric conditions (as compiled from available datasets 18) are the primary boundary conditions for this model. We rely on this work to compute the MSC-related surface load variations because of its more realistic hypsometry relative to previous models 44 and because it takes into account the environmental lapse rate, the control by precession cycles on rainfall and river input and global eustatic changes calibrated on $\delta^{18}O$ data. These models, however, differ in the details but agree on the magnitudes, therefore we expect that the model by ref. 44 would lead to similar results. The scenario proposed by ref. 25, involving a shorter time lag for the drawdown and evaporites deposition and earlier drawdown with respect to the evaporites deposition 20 based on inshore and offshore observations from the Gulf of Lions, Italy and Turkey, is also considered (Supplementary Fig. 2). Finally, we account for a “no-drawdown” scenario for the MSC 14,13 by removing the contribution to surface load variations by sea level changes from the time history proposed by ref. 18.

For each of the three representative scenarios, variations of the surface load with respect to pre-MSC conditions, $\Delta L_{s(t)}$ (Fig. 1b and Supplementary Fig. 2), are computed as:

$$\Delta L_{s(t)}=g(\rho_{w(t)}h_{w(t)}+\rho_s h_{s(t)} - \rho_{w(t_0)}h_{w(t_0)}+\rho_s h_{s(t_0)}) \quad (1)$$

where $\rho_{w(t)}$ is the time dependent mean water density, ρ_s is the mean salt density (time independent), $h_{w(t)}$ and $h_{s(t)}$ are the time dependent mean water depth and salt deposit thickness, g is the gravity acceleration, and subscript (t_0) indicates quantities at a reference time soon before the onset of the MSC. Assuming that $h_{s(t0)}$ is nil, equation (1) becomes

$$\Delta L_{s(t)}=g(\rho_{w(t)}h_{w(t)}+\rho_s h_{s(t)} - \rho_{w(t_0)}h_{w(t_0)}) \quad (2)$$

ρ_s and $\rho_{w(t0)}$ are set to 2160 kg/m^3 and 1029 kg/m^3, respectively. $\rho_{w(t)}$ (Supplementary Fig. 5) is constrained by the salinity changes estimated by ref. 18, and the equation of state for seawater by ref. 45 (the ocean water density calculator available at http://www.csgnetwork.com/water_density_calculator.html was used for this operation). We set $h_{w(t0)}$ equal to 2500 m, that is approximately the mean bathymetry of the Mediterranean in the Messinian 46. $h_{w(t)}$ is obtained by adding to this value the water surface changes (negative for lowering) provided by refs. 18 and 25, while it is assumed constant through time for the “no-drawdown” scenario. $h_{s(t)}$ is constrained by the time history of salt deposition provided by refs. 18 and 25 divided by the area of the Mediterranean basins (Fig.

Europe PMC Funders Author Manuscripts

1a and Supplementary Fig. 2). Note that the volumes of salt deposits are overestimated by not being corrected for the interleaved detritus and more appropriate values are obtained by applying a reduction by up to 75% (ref. 18). We thus compute envelopes that report on estimates of $\Delta L_{s(t)}$ accounting for a reduction of $h_{s(t)}$ by 0% (i.e., no modification of the salt volumes provided by ref. 18), 50% and 75% (Fig. 1b and Supplementary Fig. 2).

Igneous mineral ages compilation and analysis

Volumetric estimates of the magmatic products during the MSC are limited by compromised preservation due to erosion and the Plio-Quaternary tectonics. Instead, the number of volcanic and intrusive events, represented by igneous mineral ages during the time window of interest, is often used as a proxy for local, regional or global magmatic trends 1,7,47,48. We follow this approach and generate a database of published mineral ages of igneous rocks from the pan-Mediterranean area during the 6.4-5 Ma time window (Supplementary Table 1) based on careful manual literature screening (Fig. 1c, d, a full reference list is provided in Supplementary Information). Selected units are separated in space and time by at least 10 km and 10 ka, which enables avoiding bias due to multiple sampling or studies focused on particular events or regions, and a single entry is assigned to each unit. 35 entries compose our database; we remark that the number of entries per unit time, per unit area of investigation is higher than that of previous works based on a similar approach 1,7,4,47, which gives us confidence on the dataset reliability.

Age-histograms were generated to assess time variations of the magmatic activity (Fig. 1c and Supplementary Fig. 1 and 4). The bin size for the histogram in Fig. 1c (i.e., 0.3 Ma) was selected based on Scott's normal reference rule and the age measurement errors are in most cases smaller than or equal to this value (the analyses and conclusions hold if entries with age measurement error larger than this value or not provided are removed from the database). Histograms based on bin sizes of 0.2 and 0.4 Ma still show the peak of magmatism during the second half of the MSC (Supplementary Fig. 4). A histogram of data from a careful selection from the Earthchem archive (http://www.earthchem.org as of August 2016) throughout the Neogene in the Mediterranean (Supplementary Fig. 1) shows no other peaks comparable to that during the second half of the MSC, stressing the outstanding nature of this event. A histogram of data from a careful selection from the Earthchem archive (as of January 2017) throughout the 6.4-5 Ma time window worldwide shows no significant trends, which rules out global-scale forcings and indicates that the trends in Figs. 1c and Supplementary Fig. 1 are limited to the Mediterranean realm.

Exploring the magmatic effects of surface load variations

Overall, surface unloading, implying decreased lithostatic pressure at depth, enhances the production and emplacement/release of magma, while the opposite is true for surface loading. We provide hereafter more quantitative assessments as to the forcing from surface load changes on the production of magma by decompression partial mantle melting and the effects on magma reservoirs. In doing this, we account for the average relative position of the igneous provinces included in our database and salt deposits with respect to that of the basin (Fig. 1d).

Surface load changes and magma generation by decompression partial mantle melting—The magma production rate, DF/Dt, for pressure release melting at constant entropy, S, can be estimated as 2

$$\frac{DF}{Dt}=\left(\frac{\partial F}{\partial P}\right)_S\left(\frac{\partial P}{\partial t}-\overline{V}\cdot\nabla P\right) \quad (3)$$

where F is the melt fraction, P is pressure, T is temperature, t is time and $\bar{\boldsymbol{V}}$ is the mean mantle upwelling rate. At any given depth (i.e., where the term $\partial F/\partial P$ is constant), a direct comparison between the terms $\partial P/\partial t$ and $\bar{\boldsymbol{V}}\cdot\nabla P$ provides a first order assessment as to the potential relative contributions to the Mediterranean magmatism from MSC-related surface load variations and the background mantle upwelling, respectively.

Using the standard expression $P=\int\rho gdz$ to compute the lithostatic pressure at depth, z, and assuming a uniform rock density, ρ, of 3000 kg/m^3 and $\bar{\boldsymbol{V}}$ in backarc environments of up to a few centimetres per year 21, the term $\bar{\boldsymbol{V}}\cdot\nabla P$ varies in the order of the hundreds of Pa/a. With this in mind, we estimated $\partial P/\partial t$ due to MSC-related surface load variations, $\Delta L_{s(t)}$ (estimated as described in the previous section), solving the 2D Stokes, continuity and advection equations using standard finite differences and marker in cell techniques on a regular grid using pressure-velocity formulations 49. The Earth model is composed by two incompressible Maxwell viscoelastic layers (analogues for the crust and mantle) characterized by different viscosities, η_c and η_m, and elastic modulus, E_c and E_m and with relative densities of 2750 and 3300 kg/m^3. The model domain (Fig. 2) measures 3000 by 400 km in the horizontal and vertical dimensions, resolved by ~30x4 km element size and 160000 markers advected accordingly to the computed velocity field and a fourth-order Runge-Kutta scheme. Free-slip velocity boundary conditions are applied to all boundaries and an 8 km thick “sticky air” layer 49 is imposed at the top of the model domain. The upper layer is 50 km thick and characterized by a 6 km thick basin-like structure on the right hand side, whose density is varied through time to mimic a forcing comparable in magnitude and timing to $\Delta L_{s(t)}$ in Fig. 1b.

We tracked $\partial P/\partial t$ at a hypothetical magma source point located at ~60 km depth and in the proximity of (but outside) the basin-like structure (Fig. 2a), a choice driven by the fact that most rocks composing our database come from inland magmatic provinces (Fig. 1d). We found that, for common viscosities and elastic moduli 29, $\partial P/\partial t$ varies in the order of the tens of Pa/a, with peaks in the order of the hundreds of Pa/a if catastrophic events (e.g., abrupt flooding of the Mediterranean at the end of the MSC) are involved. Higher $\partial P/\partial t$ values would be obtained if the hypothetical magma source point was shallower. These predictions are consistent with results from other studies 2,50 involved with surface load changes of different origins but similar magnitudes, which gives us confidence about the validity of the assumptions embedded into our model.

The modeling shows that, although $\partial P/\partial t$ at depth is in general one order of magnitude smaller than $\bar{\boldsymbol{V}}\cdot\nabla P$, it may reach up to similar values when extreme events occur (Fig. 2a-c).

Following the analytical framework provided by ref. 5, and accordingly with equation (4), the adiabatic melt production rate due to mantle upwelling, Γ_{upw}, is

$$\Gamma_{upw}=\rho_m \overline{V} \left|\frac{\mathrm{dF}}{dy}\right|$$

where y is a coordinate aligned with gravity and positive downward. The volume of melts produced, Mv_{upw}, is obtained by depth-integration of Γ_{upw}

$$Mv_{upw}=\int_{y_m}^{y_0}\Gamma_{upw}dy=\rho_m \overline{V}\int_{y_m}^{y_0}\left|\frac{\mathrm{dF}}{dy}\right|dy \quad (4)$$

where y_0 and y_m define the Earth's surface and the maximum depth at which partial melting occurs, respectively. The perturbation from $\Delta L_{s(t)}$ to Γ_{upw}, Γ_{sl}, can be calculated as

$$\Gamma_{sl}=\frac{1}{g}\left|\frac{\mathrm{dF}}{dy}\right|\frac{\partial P}{\partial t}$$

Let us define R such that

$$R=\frac{\Gamma_{sl}}{\Gamma_{upw}}=\frac{1}{\rho_m g \overline{V}}\left(\frac{\partial P}{\partial t}\right) \quad (5)$$

being the percentage modulation of Γ_{upw} due to $\Delta L_{s(t)}$. In Fig. 2b and c, we provide an estimate of R assuming uniform and constant ρ_m = 3300 kg/m^3 and $\bar{V}$ = −1 cm/a. Note that, because negative $\bar{V}$ imply upwelling in our reference system, when the $\Delta L_{s(t)}$ is positive R is negative and vice versa. In addition, under the assumption of uniform and constant $\bar{V}$ and ρ_m, R is solely controlled by $\partial P/\partial t$. The additional volume of melts produced due to $\Delta L_{s(t)}$, Mv_{sl}, is obtained by depth-integration of Γ_{sl},

$$Mv_{sl}=\int_{y_m}^{y_0}\Gamma_{sl}dy=\frac{1}{g}\int_{y_m}^{y_0}\left|\frac{\mathrm{dF}}{dy}\right|\frac{\partial P}{\partial t}dy \quad (6)$$

In Fig. 3, this theory is applied to an equilibrium continental geotherm and a parameterization for partial mantle melting as function of pressure and temperature 26 in order to provide estimates of Γ_{upw}, Γ_{sl} and the additional magma per unit time and surface area produced during the unloading phase of the reference MSC-scenario.

In general, $\partial P/\partial t$ due to surface load variations are sustained for relatively short times outside surface loading/unloading phases because of the viscous stress relaxation. However, adiabatic loading/unloading implies instantaneous modifications of the magma production rates. Additional melts then upwell through the lithosphere at rates that may be as fast as tens of meters per year 29 and thus the newly-produced magma can migrate through a 100

km thick lithosphere in less than ~10 ka. We conclude that substantial deviations from the surface or near surface magmatic record by modulations of the background magma production rates due to MSC-related ΔL_s should be expected.

Surface load changes, overpressure of magma reservoirs and dike formation—Ref. 3 derived an equation to investigate the effects of glacial unloading on the dynamics of dyke formation assuming that a crustal magma chamber is embedded into Maxwell viscoelastic wall rocks. We adapt this formulation to our work by substituting the rate of glacial unloading term with the rate of change of surface load due to the MSC, $\partial\Delta L_s/\partial t$, and obtain

$$\frac{\partial \Delta P_{ch}}{\partial t} + \frac{E_c}{\eta_c}\Delta P_{ch} = -\frac{\partial \Delta L_s}{\partial t} \quad (7)$$

where $\Delta P_{ch} = P_{ch} - P$ is the overpressure within the magma chamber (with P_{ch} and P being the pressure within the magma chamber and the remote lithostatic stress, respectively), while E_c and η_c are the elastic modulus and viscosity of the crustal wall rock. We remark that the inherent simplifications into our geodynamic modeling prevent us from estimating P_{ch} and, therefore, the solution of equation (7) is beyond our possibilities. However, for very high η_c (e.g., $\geq 10^{23}$ Pa s), the rate of change of surface load variations (rather than the absolute magnitude) essentially controls $\partial\Delta P_{ch}/\partial t$, that is equation (7) becomes

$$\frac{\partial \Delta P_{ch}}{\partial t} = -\frac{\partial \Delta L_s}{\partial t} \quad (8)$$

Assuming that this condition applies to our geodynamic models, we use the computed $\partial P/\partial t$ as the forcing term in equation (8) (i.e., we impose $-\partial\Delta L_s/\partial t = \partial P/\partial t$) and plot $\partial\Delta P_{ch}/\partial t$ at 20 km depth, above the reference point shown in Fig. 2. Results are shown in Fig. 4a and discussed in the main text. If the viscous response is not negligible (e.g., for $\eta_c \leq 10^{22}$ Pa s), instead, E_c/η_c (i.e., the inverse Maxwell relaxation timescale, $1/\tau_m$) with respect to the timescale at which surface load variations take place, τ_{Ls} (in the order of 10^4-10^5 a for MSC-related events), defines the system response time. τ_m is estimated to be in the order of 10^4 ka or shorter for silicic dike formation and volcanism 29,3. Assuming $\Delta P_{ch} > \Delta P_{max}$, where ΔP_{max} is the maximum sustainable magma chamber overpressure, and for τ_m/τ_{Ls} smaller than ~0.1 eruptions by dyke formation is expected with a delay of ~10 ka after the forcing by surface load variations 3, that is shorter than τ_{Ls}. As such, substantial deviations from the surface or near surface magmatic record by modulations of the overpressure within magma chambers due to MSC-related ΔL_s should be expected.

Data and code availability

The data used in this work, provided in Supplementary Tab. 1, is obtained from the Earthchem archive at http://www.earthchem.org and manual literature screening. The authors declare that all data supporting the findings of this study are available within the article and its supplementary information files. The code used for the geodynamic modeling

and all related results can be requested directly to the leading author or accessed at https://sites.google.com/site/pietrosternai1/repositories/nature-geoscience-2017.

Supplementary Material

Refer to Web version on PubMed Central for supplementary material.

Acknowledgements

PS is grateful to the Swiss NSF for providing funding for this project (Ambizione grant PZ00P2_168113/1). LC and TS were funded by the European Research Council (ERC) under the European Union's Horizon 2020 research and innovation programme (grant agreement No. 677493 - FEVER). DGC was funded by the *MITE* CGL2014-59516 (Spanish Government). SC was funded by Swiss NSF grant No 200021–146822. Jean-Arthur Olive is thanked for precious suggestions regarding Fig. 3 and all related aspects.

References

1. Jicha B, Scholl DW, Rea D. Circum-Pacific arc flare-ups and global cooling near the Eocene-Oligocene boundary. Geology. 2009; 37:303–306.
2. Jull M, McKenzie D. The effect of deglaciation on mantle melting beneath Iceland. Journal of Geophysical Research. 1996; 101:21815–21828.
3. Jellinek AM, Manga M, Saar MO. Did melting glaciers cause volcanic eruptions in eastern California? Probing the mechanics of dike formation. Journal of Geophysical Research. 2004; 109:B09206.
4. Huybers P, Langmuir C. Feedback between deglaciation, volcanism, and atmospheric CO2. Earth and Planetary Science Letters. 2009; 286:479–491.
5. Crowley JW, Katz RF, Huybers P, Langmuir C, Park S-H. Glacial cycles drive variations in the production of oceanic crust. Science. 2015; 347:1237–1240. [PubMed: 25766231]
6. Sternai P, Caricchi L, Castelltort S, Champagnac J-D. Deglaciation and glacial erosion: a joint control on magma productivity by continental unloading. Geophysical Research Letters. 2016; 43doi: 10.1002/2015GL067285
7. McGuire WJ, et al. Correlation between rate of sea-level change and frequency of explosive volcanism in the Mediterranean. Nature. 1997; 389:473–476.
8. Gautier F, Clauzon G, Suc JP, Cravatte J, Violanti D. Age et durée de la crise de salinité messinienne. C R Acad Sc. 1994; 318:1103–1109.
9. Hsü KJ, Ryan WB, Cita M. Late Miocene desiccation of the Mediterranean. Nature. 1973; 242:240–244.
10. Ogniben L. Petrografia della Serie Solfifera Siciliana e considerazioni geologiche relative. Mem Descr Carta Geol Ital. 1957; 22:1–275.
11. Perrodon A. Etude géologique des bassins néogènes sublittoraux de l'Algérie occidentale. Bull Serv Carte Géol Algér. 1957; 12:328.
12. Clauzon G, Suc JP, Gautier F, Berger A, Loutre MF. Alternate interpretation of the Messinian salinity crisis: Controversy resolved? Geology. 1996; 24:363–366.
13. Roveri M, et al. Dense shelf water cascading and Messinian canyons: a new scenario for the Mediterranean salinity crisis. American Journal of Science. 2014; 314:751–784.
14. Lugli S, Manzi V, Roveri M, Schreiber B. The deep record of the Messinian salinity crisis: Evidence of a non-desiccated Mediterranean Sea. Palaeogeography, Palaeoclimatology, Palaeoecology. 2015; 297:83–99.
15. Urgeles R, et al. Newconstraints on the Messinian sealevel drawdown from3D seismic data of the Ebro Margin, western Mediterranean. Basin Research. 2011; 23:123–145.
16. Roveri R, et al. The Messinian salinity crisis: Past and future of a great challenge for marine sciences. Marine Geology. 2014; 352:25–58.

17. Hsü, KJ., Cita, M., Ryan, B. The origin of the Mediterranean evaporites. Initial Reports of the Deep Sea Drilling Project. Ryan, WFB.Hsü, KJ., et al., editors. Vol. 13. 1973. p. 1203-1231.
18. Ryan WB. Modeling the magnitude and timing of evaporative drawdown during the Messinian salinity crisis. Stratigraphy. 2008; 5:227–243.
19. Ryan WB, Cita MB. The nature and distribution of Messinian erosional surfaces—Indicators of a several-kilometer-deep Mediterranean in the Miocene. Marine Geology. 1978; 27:193–230.
20. Ryan WB. Geodynamic responses to a two-step model of the Messinian salinity crisis. Bull Soc géol Fr. 2011; 182:73–78.
21. Jolivet L, Augier R, Robin C, Suc JP, Rouchy JM. Lithospheric-scale geodynamic context of the Messinian salinity crisis. Sedimentary Geology. 2006; 188-189:9–33.
22. Duggen S, Hoernle K, van den Bogaard P, Harris C. Magmatic evolution of the Alboran region: the role of subduction in forming the western Mediterranean and causing the Messinian Salinity Crisis. Earth and Planetary Science Letters. 2004; 218:91–108.
23. Jolivet L, Brun J-P. Cenozoic geodynamic evolution of the Aegean. International Journal of Earth Sciences. 2010; 99:109–138.
24. Serri GF, Innocenti F, Manetti P. Geochemical and petrological evidence of the subduction of delaminated Adriatic continental lithosphere in the genesis of the Neogene–Quaternary magmatism of Central Italy. Tectonophysics. 1993; 223:117–147.
25. Bache F, et al. A twostep process for the reflooding of the Mediterranean after the Messinian Salinity Crisis. Basin Research. 2012; 24:125–153.
26. Ghiorso MS, Hirschmann MM, Reiners PW, Kress VC. The pMELTS: A revision of MELTS for improved calculation of phase relations and major element partitioning related to partial melting of the mantle to 3 GPa. Geochemistry, Geophysics, Geosystems. 2002; 3:1–35.
27. Tumanian M, Frezzotti ML, Peccerillo A, Brandmayr E, Panza G. Thermal structure of the shallow upper mantle beneath Italy and neighbouring areas: Correlation with magmatic activity and geodynamic significance. Earth-Science Reviews. 2012; 114:369–385.
28. Jolivet L, et al. Ductile extension in alpine Corsica. Geology. 1990; 18:1007–1010.
29. Turcotte, DL., Schubert, G. Geodynamics. Cambridge University Press; Cambridge: 2002.
30. Turcotte DL, Ahern JL. A porous flow model for magma migration in the asthenosphere. Journal of Geophysical Research. 1978; 83:767–772.
31. Rubin AM. Tensile fracture of rock at high confining pressure: Implications for dike propagation. Journal of Geophysical Research. 1993; 98:15919–15935.
32. Olive J-A, et al. Sensitivity of seafloor bathymetry to climate-driven fluctuations in mid-ocean ridge magma supply. Science. 2015; 350:310–313. [PubMed: 26472905]
33. Gargani J, Rigollet C. Mediterranean Sea level variations during the Messinian salinity crisis. Geophysical Research Letters. 2007; 34:10.
34. Garcia-Castellanos D, Villaseñor A. Messinian salinity crisis regulated by competing tectonics and erosion at the Gibraltar arc. Nature. 2011; 480:359–363. [PubMed: 22170684]
35. Jolivet L, Faccenna C. Mediterranean extension and the Africa-Eurasia collision. Tectonics. 2000; 19:1095–1106.
36. Krijgsman W, Garcés M. Paleomagnetic constraints on the geodynamic evolution of the Gibraltar Arc. Terra Nova. 2004; 16:281–287.
37. Malinverno A, Ryan WB. Extension in the Tyrrhenian Sea and shortening in the Apennines as result of arc migration driven by sinking of the lithosphere. Tectonics. 1986; 5:227–245.
38. Jolivet L, et al. Subduction, convergence and the mode of backarc extension in the Mediterranean region. Bull Soc géol Fr. 2008; 179:525–550.
39. Duggen S, Hoernle K, Van Den Bogaard P, Rüpke L, Morgan JP. Deep roots of the Messinian salinity crisis. Nature. 2003; 422:602–606. [PubMed: 12686997]
40. Pe-Piper, G., Piper, DJ. Unique features of the Cenozoic igneous rocks of Greece. Postcollisional tectonics and magmatism in the Mediterranean region and Asia, Geological Society of America. Dilek, Y., Pavlides, S., editors. 2006. p. 259-282.
41. Jolivet L, et al. The geological signature of a slab tear below the Aegean. Tectonophysics. 2015; 659:166–182.

42. Sternai P, Jolivet L, Menant A, Gerya T. Driving the upper plate surface deformation by slab rollback and mantle flow. Earth and Planet Sci Lett. 2014; 405:110–118.
43. Menant A, Sternai P, Jolivet L, Guillou-Frottier L, Gerya TV. 3D numerical assessments for mantle flow and magma genesis in laterally constrained subduction zones: the eastern Mediterranean case study. Earth and Planetary Science Letters. 2016; 442:93–107.
44. Blanc PL. Of sills and straits: a quantitative assessment of the Messinian Salinity Crisis. Deep Sea Research Part I: Oceanographic Research Papers. 2000; 47:1429–1460.
45. Millero F, Chen C, Bradshaw A, Schleicher K. A new high pressure equation of state for seawater. Deep Sea Research, Part A. 1980; 27:255–264.
46. Govers R. Choking the Mediterranean to dehydration: the Messinian salinity crisis. Geology. 2009; 37:167–170.
47. von Blanckenburg F, Huw Davies J. Slab breakoff: A model for syncollisional magmatism and tectonics in the Alps. Tectonics. 1995; 1:120–131.
48. McKenzie NR, et al. Continental arc volcanism as the principal driver of icehouse-greenhouse variability. Science. 2016; 352:444–447. [PubMed: 27102480]
49. Gerya, T. Introduction to Numerical Geodynamic Modelling. Cambridge University Press; 2010.
50. Schmidt P, et al. Effects of present-day deglaciation in Iceland on mantle melt production rates. Journal of Geophysical Research: Solid Earth. 2013; 118:3366–3379.

Europe PMC Funders Author Manuscripts

Europe PMC Funders Author Manuscripts

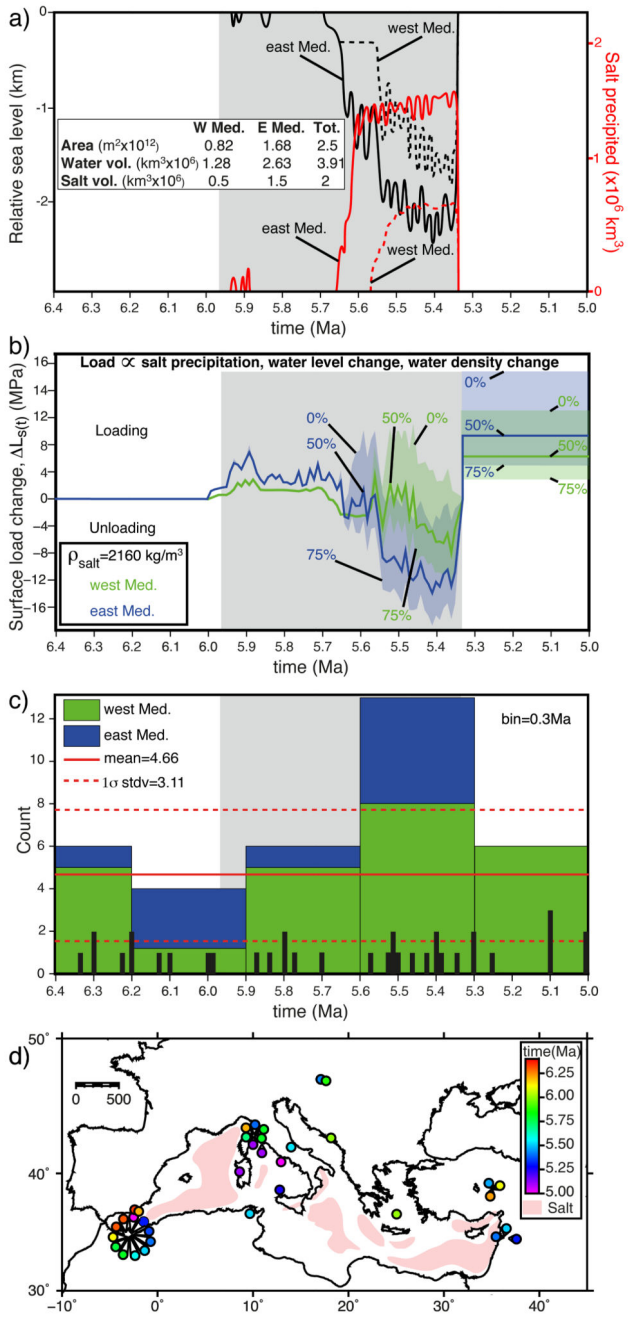

Figure 1. Distribution of Mediterranean magmatic minerals dated between 5-6.4 Ma and surface load variation estimates by the reference MSC scenario.

(a) Relative sea level and salt precipitation (ref. 18), the inset provides values to convert salt volumes into average thickness. (b) $\Delta L_{s(t)}$ (i.e., surface load changes,) estimated from the curves in panel a and Supplementary Fig. 5. The 0%, 50% and 75% curves show $\Delta L_{s(t)}$ after reducing the salt volume by that amount to account for interleaved sediments. (c) Mineral age histogram (black bars show the distribution). Red lines show the time-averaged count and the 1σ standard deviation. (d) Sample ages and locations and distribution of major salt deposits. The grey bar in panels a-c highlights the MSC.

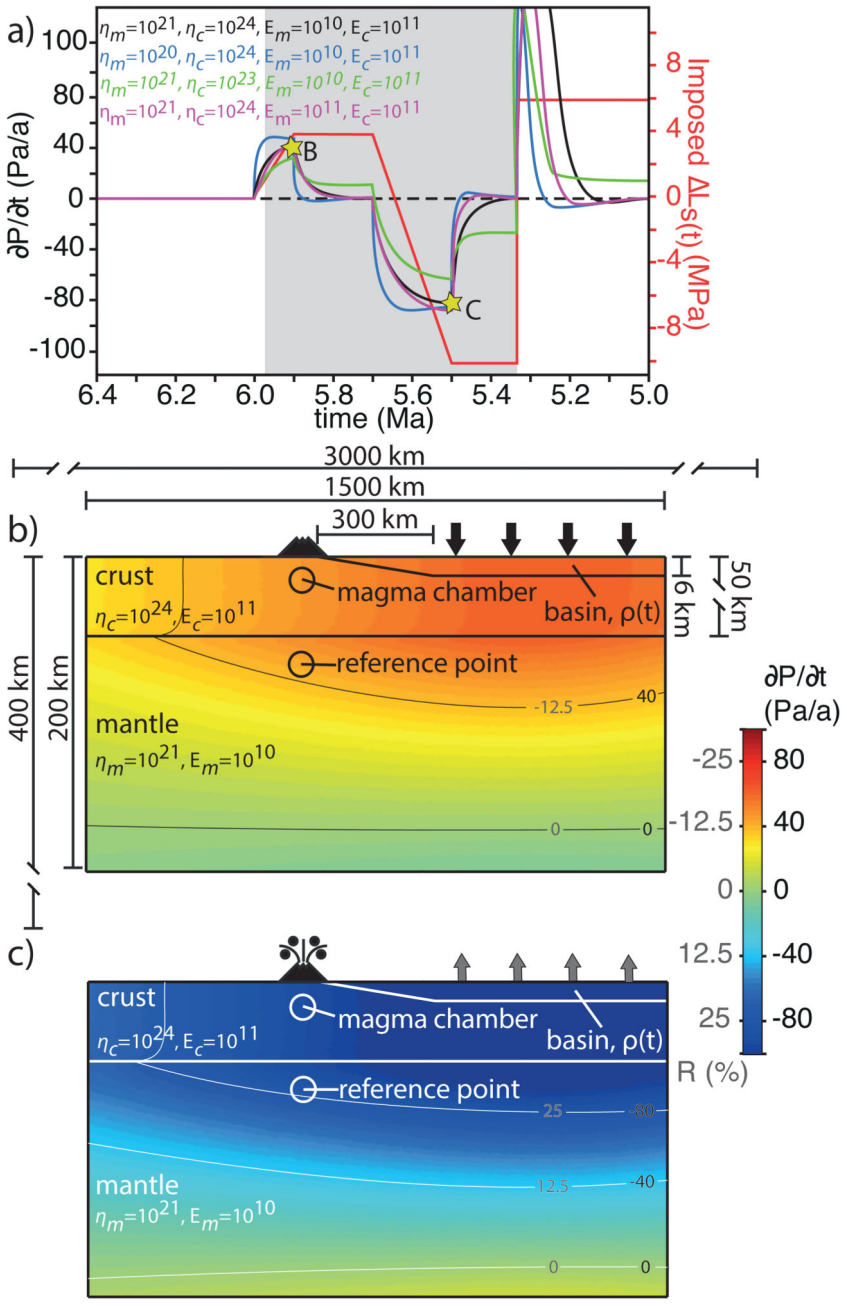

Figure 2. Pressure and melt production change rate at depth in response to the MSC-related surface load variations.

(a) The red curve shows the imposed surface load variations, mimicking the MSC-related surface load change, $\Delta L_{s(t)}$ (Fig.1b). The other curves show the parametric study on the viscosity, η_c and η_m, and elastic modulus, E_c and E_m, of the upper and lower layers (analogue for the crust and mantle, respectively). Curves are computed at the reference point shown in panels b and c. The grey bar highlights the MSC. (b, c) $\partial P/\partial t$ and

$R_{(t)}=\frac{1}{\rho_m \overline{\overline{g}}\,\overline{\overline{V}}}\left(\frac{\partial P}{\partial t}\right)$ (see Methods) at the time-step shown by the stars in panel a. $\Delta L_{s(t)}$ is imposed by modulating the density of the material within the basin-like structure.

Europe PMC Funders Author Manuscripts

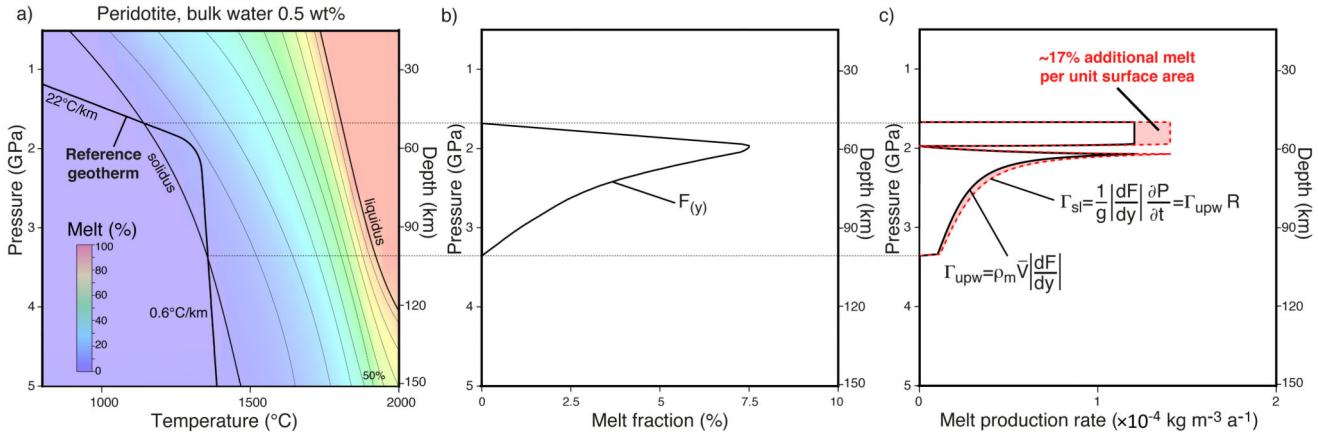

Figure 3. Partial melting of partially hydrated mantle rocks modulated by surface unloading.

(a) Equilibrium melt percentage of a peridotite (calculations based on MELTS, ref. 26). Initial rock composition: SiO_2-45.47%, TiO_2-0.11%, Al_2O_3-4%, Fe_2O_3-0.585%, Cr_2O_3-0.68%, FeO-6.696%, MgO-38.53%, CaO-3.59%, MaO-0.31%, H_2O-0.5%. The thick black line shows a reference geotherm. (b) Melt fraction vs. depth/pressure for the reference geotherm. (c) Melt production rate vs. depth/pressure at equilibrium conditions (black curve) and after correction by R in Fig. 2c, along the vertical through the reference point (dashed red curve). We assume uniform and constant ρ_m = 3300 kg/m^3 and $\bar{V}$ = 1 cm/a, see also the Methods section.

Europe PMC Funders Author Manuscripts

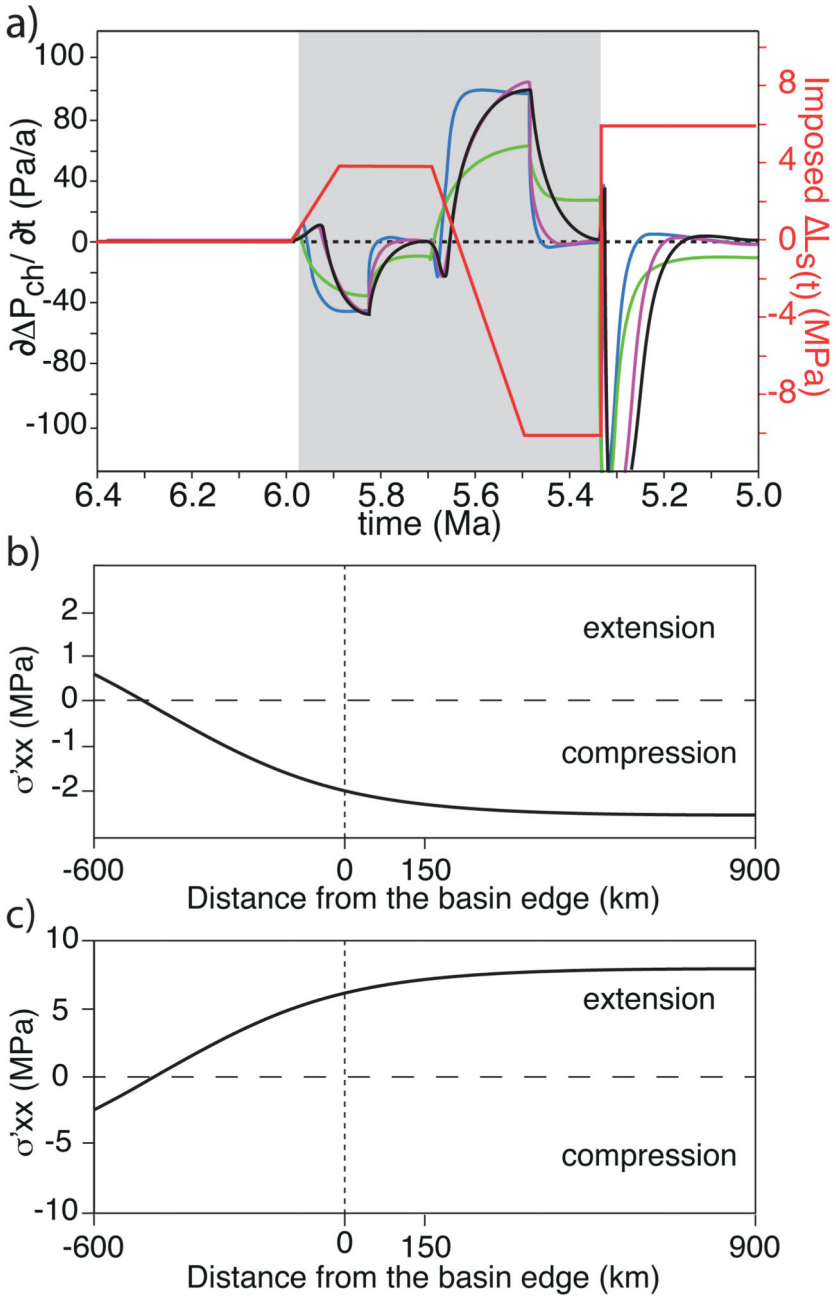

Figure 4. Overpressure and deviatoric horizontal stresses for the geodynamic model in Fig. 2.

(a) Temporal variations of the overpressure within a hypothetical magma chamber at 20 km depth, above the reference point (shown in Fig. 2b, c). The colour scheme is the same as in Fig. 2a. (b, c) Deviatoric horizontal stress, σ'_{xx}, at 20 km depth for the model time-steps shown in Fig. 2b, c, respectively. The horizontal distance is relative to the edge of the basin-like structure (vertical dashed line). Note that crustal levels below and nearby the basin-like

structure are subject to slight horizontal compression and extension during the loading and unloading phase, respectively.

Europe PMC Funders Author Manuscripts